Dynamics of ultrafast magnetization reversal in submicron elliptical Permalloy thin film elements

Q. F. Xiao,[1] J. Rudge,[1] B. C. Choi,[1] Y. K. Hong,[2] and G. Donohoe[3]
[1]*Department of Physics and Astronomy, University of Victoria, Victoria, BC, Canada V8W 3P6*
[2]*Department of Materials Science and Engineering, University of Idaho, Moscow, Idaho 83844, USA*
[3]*Department of Electrical and Computer Engineering, University of Idaho, Moscow, Idaho 83844, USA*
(Received 26 October 2005; revised manuscript received 22 December 2005; published 20 March 2006)

The micromagnetic dynamics of ultrafast magnetization reversal in elliptical Permalloy ($Ni_{80}Fe_{20}$) thin film elements is described. It is shown that coherent rotation and magnetization ringing in submicron Py elements can be controlled by adjusting the axis ratio of the ellipse, the thickness, and the angle of the magnetic field pulse. For the elliptical Py element with 400-nm-long axis, 200-nm-short axis, and 4.7 nm thickness, the nonuniform distribution of magnetization results from a strong in-plane, nonuniform demagnetization field during magnetization precession. It is the main reason magnetization ringing appears, even though the average values of M_y and M_z are equal to zero at the moment the pulse is terminated. The simulation results indicate that uniformity in the distribution of the magnetization during reversal is improved by reducing the length of the short axis from 200 to 112 nm, and reducing the thickness of the thin film from 4.7 to 3.2 nm. The modification in the geometric configuration of the element is found to effectively suppress the magnetization ringing.

DOI: 10.1103/PhysRevB.73.104425 PACS number(s): 75.40.Gb, 75.40.Mg, 75.50.Ss, 75.60.Jk

I. INTRODUCTION

The factors impacting magnetization reversal in a magnet can be categorized as either intrinsic or extrinsic. Intrinsic factors are, for example, composition and crystal structure that determine properties such as the saturation magnetization M_s, the exchange interaction constant A, and the magnetocrystalline anisotropy constant K_a. The roughness of crystal boundaries and surfaces and interfaces, the density and orientation of steps, strains, texture, dislocation, and defects are collectively referred to as a magnet's microstructure. The microstructure is another intrinsic factor that seriously affects the magnetic properties of a magnet. Less obvious intrinsic factors are the size and shape of a magnet. These strongly influence the distribution of magnetization $\mathbf{M}$ and demagnetization field $\mathbf{H_d}$, and the magnetic domains in both the static equilibrium state (i.e., before and after magnetization reversal) and during the process of magnetization reversal. The practical control of these factors is the subject of numerous experimental and theoretical problems.[1–7] Of the extrinsic factors, the effects of the external surroundings on the magnet, the most notable is the external field. Its strength, rise time, fall time, duration, and orientation all play key roles in the dynamic process of magnetization reversal. Design of an appropriate external magnetic field pulse involves some technical problems and is usually done by experimental methods. Another extrinsic factor worth noting is the temperature, which is important during magnetization reversal.[1]

The advantage of a giant magnetic resistance or a magnetic tunneling junction based system for magnetic random access memory, as well as any other magnetic storage device, is that it would have a quicker write time and be more energy efficient. To obtain the fastest magnetization reversal, the ideal mechanism is a complete, coherent, rotation of the magnetization without forming any magnetic domain walls within the element. Since domain wall motion requires more time to complete the magnetization reversal, avoiding domain wall formation, and the subsequent motion of those walls, the magnetization reversal is faster. On the other hand, a higher normalized remanence and a modest high coercivity are required for magnetic storage elements to guarantee the accuracy and stability of the data. How to obtain both the fastest magnetization reversal and a stable magnetization after reversal in small magnetic elements is a very worthwhile topic in ultrafast magnetization dynamics and in ultrahigh density magnetic recording media. Many studies have been done on this subject by numerical simulation and experiment.[2–7] Among the more successful results was a complete magnetization reversal at about 200 ps without any further magnetization precession or magnetization ringing. This was accomplished in an 8 nm thin Py element with elliptical shape (16 μm$\times$8 μm) using a 70 Oe, transverse, shaped magnetic field pulse which was cut off at the appropriate time.[3] With the development of (and advances made in) electron beam lithography, the fabrication of magnetic elements smaller than a 100 nm is relatively easy. Clearly, a smaller element would allow for higher density applications, but when the size of the magnetic element is reduced to submicron dimensions, it has been found impossible to obtain a complete, coherent rotation without magnetization ringing using the previous method. The present work demonstrates simulation studies that yield a solution to the problem. In the simulation, run on OOMMF software,[8] both ultrafast magnetization reversal and suppression of the magnetization ringing were obtained in an elliptical element of Py thin film with submicron dimensions. The axis ratio of the ellipse, the thickness of the thin film, the orientation and the duration time of the magnetic field pulse were varied throughout the studies.

II. MICROMAGNETIC SIMULATION MODEL

The Landau–Lifshitz–Gilbert (LLG) equation, $d\mathbf{M}(t)/dt = -|\gamma|[\mathbf{M}(t)\times\mathbf{H_{eff}}(t)] - \lambda\{\mathbf{M}(t)\times[\mathbf{M}(t)\times\mathbf{H_{eff}}(t)]\}$, is a phe-

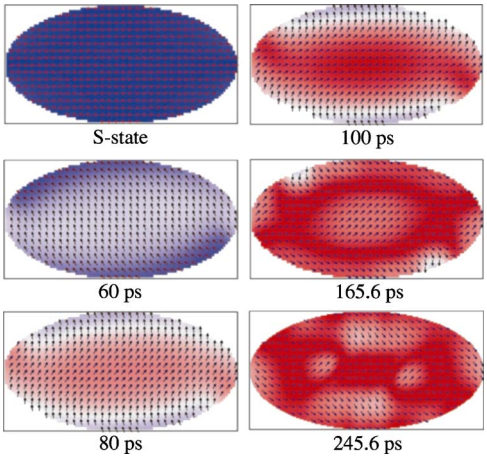

FIG. 1. (Color online) Domain configurations captured at selected time points for Py ellipse with size of 400 nm×200 nm ×4.7 nm. Images represent the magnetization component along the x axis (M_x).

nomenological description of magnetization dynamics.[9] Here the gyroscopic constant γ represents the precessional frequency, and the phenomenological damping factor λ drives the system towards an energy minimum after stopping energy input to a system, i.e., energy relaxation. In general, λ is small compared to γ/M_s (where M_s is the saturation magnetization), which implies that the energy relaxation of the system takes much longer than a few full precessional cycles of magnetization **M**. This under-damped behavior is the magnetization ringing previously mentioned. The $\mathbf{H_{eff}}$ is the internal effective magnetic field of a system. Generally, the total energy density ε_{tot} in a system mainly includes Zeeman energy ε_z when an external magnetic field is applied on the system, exchange interaction energy ε_{ex}, magnetocrystalline anisotropic energy ε_{ani} and demagnetization energy ε_d, i.e., $\varepsilon_{\text{tot}}=\varepsilon_z+\varepsilon_{\text{ex}}+\varepsilon_{\text{ani}}+\varepsilon_d$. All these energies are the function of magnetization distribution **M**, i.e., $\varepsilon_i=\varepsilon_i(\mathbf{M})$. The change of each energy with respect to magnetization **M** represents the corresponding magnetic field $\mathbf{H_i}$, $(H_i=-d\varepsilon_i/dM)$. Therefore, the $\mathbf{H_{eff}}$ is the vector sum of the applied external field $\mathbf{H_{app}}$, the exchange interaction $\mathbf{H_{ex}}$, the magnetocrystalline anisotropy field $\mathbf{H_{ani}}$, and the demagnetizing field $\mathbf{H_d}$, i.e., $\mathbf{H_{eff}}=\mathbf{H_{app}}+\mathbf{H_{ex}}+\mathbf{H_{ani}}+\mathbf{H_d}$. Since the coherent rotation reversal time is very short compared with the energy relaxation time, the precessional motion of the magnetization vector is primarily governed by the first term of the LLG equation. From the LLG equation, the dynamic magnetization equilibrium condition, which is $d\mathbf{M}(t)/\mathbf{dt}=0$ [or $\mathbf{M}(t)\times\mathbf{H_{eff}}(t)=0$], can be obtained. It means that the condition for stopping magnetization precession is $\mathbf{H_{eff}}=\mathbf{0}$, or the angle between **M** and $\mathbf{H_{eff}}$ must equal 0° or 180°.

In our study, submicron, ellipse, Py thin film elements were chosen. In order to avoid magnetization reversal in the direction perpendicular to the plane of the thin film, which would form a Bloch wall, the thickness of Py thin film must be smaller than the exchange interaction length. Due to the zero magnetocrystalline anisotropy, the exchange interaction length of Py depends only on the equilibrium condition

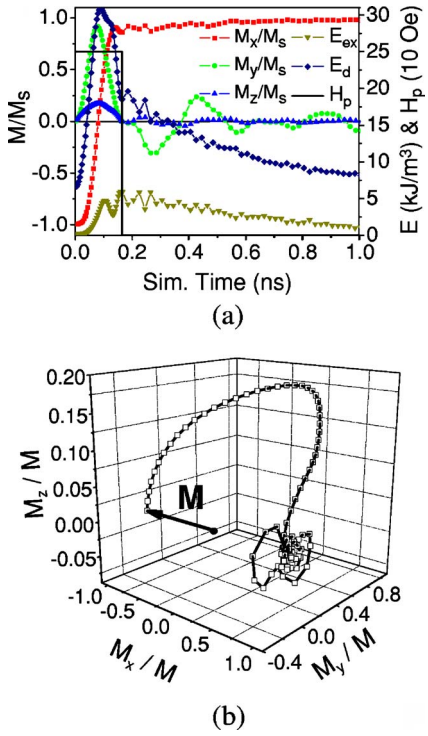

FIG. 2. (Color online) (a) Temporal evolution of the average values of the three magnetization components, the demagnetization energy E_d, the exchange energy E_{ex}, and the magnetic field pulse H_p at the angle of 55° for Py ellipse with size of 400 nm×200 nm ×4.7 nm. (b) Three-dimensional trajectory of the average magnetization **M**.

between its exchange interaction energy and its demagnetization energy. For the Py thin film, the exchange interaction length is $\Lambda=(2A/\mu_0 M_s^2)^{1/2}$.[2] For Py, $\Lambda\approx 5.29$ nm is obtained using $A=13\times10^{-12}$ J/m and $M_s=860$ kA/m.[9] On the other hand, the fundamental magnetic properties might be changed for the thickness of being smaller than 3 nm,[10,11] therefore, the thickness was varied from 5 to 3 nm. The length of long axis was fixed at 400 nm. The length of short axis was also systematically varied from 200 to 100 nm. Considering that a too small length of short axis of ellipse might lead to the increase of magnitude of magnetic field pulse to reverse magnetization, in practice the magnitude of pulse would be less than 300 Oe,[12] we reduce the length of short axis only down to 100 nm. The damping coefficient 0.01 of Py was chosen. The initial magnetization state was a saturation remnant state in the negative x direction (i.e., initially in the S state). The magnitude of the uniform magnetic field pulse was fixed at 250 Oe and the zero rise time and fall time of pulse were chosen. To suppress ringing, the magnetic field pulse was applied in the plane of the thin film (x-y plane) at a variable angle Φ relative to the long axis of the ellipse, so that the remanent energy as small as possible was obtained at the moment of cutting off the pulse and the magnetization $\mathbf{M_y}=\mathbf{M_z}=0$. In order to avoid large errors from the in-plane exchange interaction, a cell size of 2 nm×2 nm was chosen.

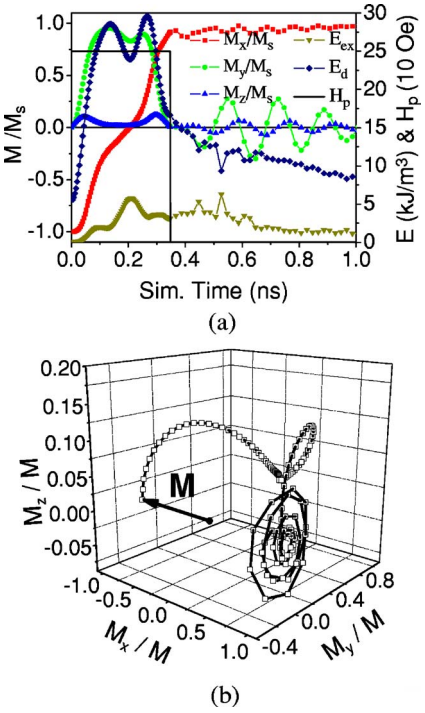

FIG. 3. (Color online) Reducing the length of the elliptical short axis from 200 to 112 nm leads to the decrease in the M_z and the backward rotation in the central part. (a) Temporal evolution of the average values of the M_x/M_s, M_y/M_s, M_z/M_s, E_d, E_{ex} and the pulse H_p at an angle of 64°. (b) Three-dimensional trajectory of average magnetization **M**.

III. RESULTS AND DISCUSSION

Figure 1 and Figs. 2(a) and 2(b) show the simulation results of the elliptical element with a 400-nm-long axis, a 200-nm-short axis, and a 4.7 nm thickness. In this case, the magnetic field pulse is applied at an angle of 55° with respect to the x-axis. Figure 1 shows the magnetization distribution at different times during the reversal. The distribution is quite uniform in the initial state, but the distribution quickly becomes nonuniform during the rotational process. The rotation of the magnetization in the outer (marginal) areas is lagging behind the central area. This indicates that the demagnetization field $\mathbf{H_{dy}}$ in these areas is larger than that in the central area. Then, the torque, $-|\gamma|[\mathbf{M}(t)\times\mathbf{H_{dy}}(t)]$, forces the magnetization **M** to rotate in the negative z direction. It follows that M_z or $\mathbf{H}_{dz}$ in these areas is smaller than in the central area. The torque, $-|\gamma|[\mathbf{M}(t)\times\mathbf{H}_{dz}(t)]$, determines the rotational speed of magnetization, therefore we can conclude that the nonuniform distribution of magnetization results from the larger demagnetization field, $\mathbf{H_{dy}}$, in the outer areas.

Figure 2(a) shows the temporal evolution of the average values of the normalized magnetization components (M_x/M_s, M_y/M_s, and M_z/M_s), the demagnetization energy E_d, the exchange energy E_{ex}, and the magnetic field pulse H_p, respectively. Although the average values $M_y/M_s=M_z/M_s=0$ at 165.6 ps, the average value of M_x/M_s is 0.86 and it has a higher E_d and E_{ex} relative to the relaxation state. From the image of the magnetization distribution at 165.6 ps in Fig. 1 it can be seen that the magnetization vectors are not perfectly

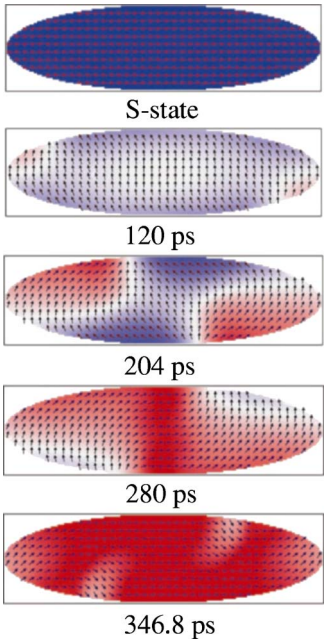

FIG. 4. (Color online) Evolution of domain configurations with increasing time for Py ellipse with size of 400 nm×112 nm ×4.7 nm. Images represent the magnetization component along the x axis (M_x).

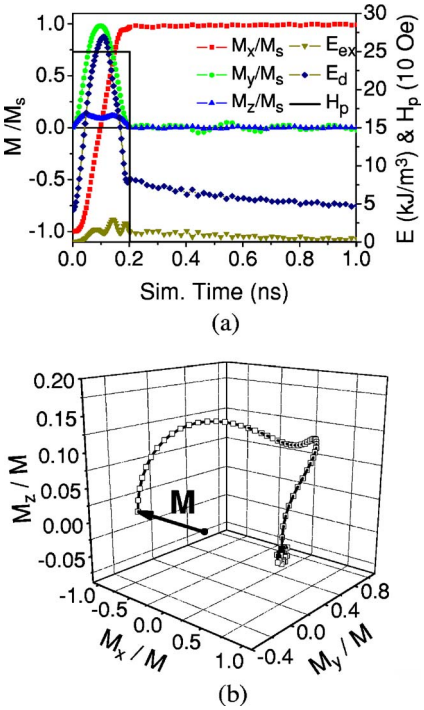

FIG. 5. (Color online) Simultaneously reducing both the length of the elliptical short axis and the thickness of thin film (400 nm ×112 nm×3.2 nm) results in a more uniform distribution of the magnetization. (a) Temporal evolution of the average values of M_x/M_s, M_y/M_s, M_z/M_s, E_d, E_{ex} and the pulse H_p at an angle of 78°. (b) Three-dimensional trajectory of the average magnetization **M**.

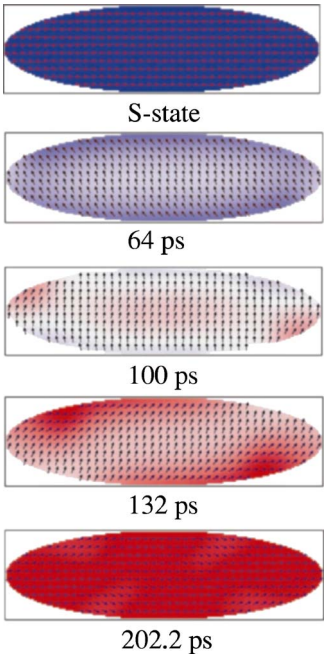

FIG. 6. (Color online) Evolution of domain configurations as a function of time for the Py ellipse with size of 400 nm × 112 nm × 3.2 nm. Images represent the magnetization component along the x axis (M_x).

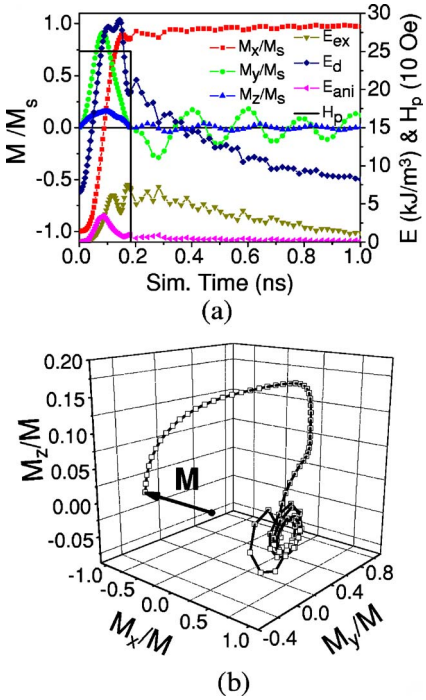

FIG. 7. (Color online) (a) Temporal evolution of the average values of the three magnetization components, the demagnetization energy E_d, the exchange energy E_{ex} the magnetic anisotropy energy E_{ani}, and the magnetic field pulse H_p at the angle of 49.6°, calculated for Py ellipse with size of 400 nm × 200 nm × 4.7 nm and K_u=3.9 kJ/m^3, (b) Three-dimensional trajectory of the average magnetization **M**.

aligned along the positive x direction. As a result, when the pulse is cut off at this time, the magnetizations in each part are not at the dynamic equilibrium state, so that the ringing around the x axis appears and persists for a longer time, as in Figs. 2(a) and 2(b). [Note the enlargement of the z-axis scale in (b).] The conclusion obtained from the result is that a uniform distribution of magnetization in the entire element during precession is the key to suppression of the magnetization ringing.

Inspection of the images at 80 and 100 ps in Fig. 1 clearly shows that the rotational delay occurs at the top and bottom arcs of the ellipse. Thus we tried to further reduce the length of short axis of the ellipse in order to flatten the top and bottom arcs which led to the nonuniform distribution. Figure 3 shows the simulation results of the elliptical element with dimensions of 400 nm × 112 nm × 4.7 nm. In Figs. 3(a) and 3(b), it can be seen that there is a cave part for the average value of M_z/M_s, M_y/M_s, and E_d, in the middle of the precessional process. In addition, the reversal speed clearly slows down. These indicate that the magnetization in some parts rotates toward the negative z direction because of the strong torque, $-|\gamma|[\mathbf{M(t)}\times\mathbf{H_{dy}}(t)]$, and with $-\mathbf{M}_z$, even rotate back towards the negative x direction. Comparing the image in Fig. 4 at 120 ps with that of Fig. 1 at 80 ps, it can be seen that the distribution of magnetization in the middle region is more uniform in Fig. 4 than that in Fig. 1. The rotational speed in Fig. 4 is clearly slower in the middle than at the left and right sides, so that the two domain walls are formed. As the reversal progresses, the domain walls move toward the middle region and the magnetizations in the middle region rotate backward, as shown in the image captured at 204 ps. Therefore, according to the dynamic principle, it can be inferred that as a result of the stronger torque $-|\gamma|[\mathbf{M}(t)\times\mathbf{H_{dy}}(t)]$, which is against the torque $-|\gamma|[\mathbf{M}(t)\times\mathbf{H_p}]$, the magnetizations in the middle region have $-M_z$ around this time, whereas the left and right sides have magnetizations of $+M_z$ and certainly rotate in the positve x direction. This should be attributed to the weaker torque $-|\gamma|[\mathbf{M}(t)\times\mathbf{H_{dy}}(t)]$ in both parts. In the two domain walls the magnetization has a large angle change in both the x-y plane and in the z direction. This large angle change leads to the higher exchange interaction energy corresponding to the maximum of E_{ex} in Fig. 3(a). As the rotation proceeds, the angles between the magnetization vectors and the y direction are increasing, so that H_{dy} and the average value of E_d are decreasing. Thus, the magnetization in the middle region rotates in the positive z and y directions again because the torque, $-|\gamma|[\mathbf{M}(t)\times\mathbf{H_p}]$ is becoming dominant again. This can be seen in Figs. 3(a) and 3(b) as an increase in M_z/M_s, M_y/M_s, E_d, and the reversal speed. Finally, the action of the two dominant torques, $-|\gamma|[\mathbf{M}(t)\times\mathbf{H_p}]$ and $-|\gamma|[\mathbf{M}(t)\times\mathbf{H_{dz}}(t)]$ cause the magnetizations in different parts to rotate toward the positive x direction, so that the average values of M_z/M_s, and M_y/M_s go down to zero at the time the pulse is terminated. In this case the distribution of the magnetization was still not uniform. By comparison with the previous elliptical element, the increase of ringing in the z direction is due to the increase of H_{dy} in this element with a shorter short axis. In order to prevent a large rotation of the magnetization in the z direction thereby increasing the uniformity of the

magnetization distribution, the thickness of the thin film was properly reduced to increase the demagnetization field in z direction.

Figure 5 and Fig. 6 show the simulation results of the elliptical element with dimensions of 400 nm $\times$ 112 nm $\times$ 3.2 nm. Comparison with the results from the last element shows that the rotation of the magnetization in the z direction is clearly suppressed by reducing the thickness of the thin film. This leads to a more uniform distribution of the magnetization during the precessional process. At 202 ps, the $M_y/M_s = M_z/M_s = 0$, M_x/M_s reaches 0.97, and both the demagnetization energy E_d and the exchange interaction energy E_{ex} are clearly smaller than those of the former two elements. This means that most of the magnetization is aligned with the positive x axis and meets the dynamic equilibrium condition at that moment, so that the ringing is largely suppressed after the magnetic field pulse is cut off.

From the results of suppressing ringing shown above, the reduction in the length of short axis and the thickness of the thin film not only increases the effective magnetic anisotropy, more importantly, it increases the uniformity of the magnetization distribution during the reversal process, so that the more uniform distribution of magnetization and lower exchange and demagnetization energy can be obtained. In literatures, several methods have been reported to increase the induced magnetic anisotropy of Py thin film.[13–15] For example, the strain induced magnetic anisotropy can give rise to the magnetic anisotropy field of Py thin film up to 92 Oe.[15] Figures 7(a) and 7(b) show the simulation results of the elliptical element with 400-nm-long axis, 200-nm-short axis, 4.7 nm thickness, and the magnetic anisotropy constant of $\mathbf{K_u} = 3.9\ \mathrm{kJ/m^3}$, which was estimated from the value of the anisotropy field given in Ref. 15. Comparing with the results in Figs. 2(a) and 2(b), the ringing cannot be suppressed by only increasing magnetic anisotropy. This result indicates that the modification of the element shape and thickness for a given material is an effective way to suppress the magnetization ringing.

IV. SUMMARY

In elliptical Py thin film elements, the nonuniform distribution of magnetization results from a stronger, in-plane, nonuniform demagnetization field during the magnetization precession. It is the main reason magnetic ringing appears, even when the average values of M_y and M_z equal zero at the moment the pulse is cut off. For the Py elliptical element with 400-nm-long axis, 200-nm-short axis, and 4.7 nm thickness, the simulation results indicate that uniformity in the distribution of demagnetization field during magnetization reversal can be improved by reducing the length of short axis from 200 to 112 nm, and simultaneously reducing the thickness of the thin film from 4.7 to 3.2 nm. The improved uniformity of magnetization during magnetization reversal effectively suppresses magnetization ringing.

ACKNOWLEDGMENTS

This work was supported by the Natural Sciences and Engineering Research Council (NSERC) of Canada and U.S. Air Force Research Laboratory (AFRL) under Grant No. F29601-04-1-206.

[1] E. Beaurepaire, M. Maret, V. Halté, J.-C. Merle, A. Daunois, and J.-Y. Bigot, Phys. Rev. B **58**, 12134 (1998).
[2] J. Miltat, G. Albuquerque, and A. Thiaville, in *Spin Dynamics in Confined Magnetic Structures I, Topics Appl. Phys.* (Springer, Berlin, 2002), Vol. 83.
[3] Th. Gerrits, H. A. M. van den Berg, J. Hohlfeld, L. Bar, and T. Rasing, Nature (London) **418**, 509 (2002).
[4] M. Bauer, J. Fassbender, B. Hillebrands, and R. L. Stamps, Phys. Rev. B **61**, 3410 (2000).
[5] M. Bauer, R. Lopusnik, J. Fassbender, and B. Hillebrands, Appl. Phys. Lett. **76**, 2758 (2000).
[6] S. Kakaa and S. E. Russek, Appl. Phys. Lett. **80**, 2958 (2002).
[7] H. W. Schumacher, C. Chappert, P. Crozat, R. C. Sousa, P. P. Freitas, J. Miltat, J. Fassbender, and B. Hillebrands, Phys. Rev. Lett. **90**, 017201 (2003).
[8] M. J. Donahue and D. G. Porter, OOMMF User's Guide, Version 1.0, National Institute of Standards and Technology (Sept. 1999), http://math.nist.gov/oommf/.
[9] L. Landau and E. Lifshitz, Phys. Z. Sowjetunion **8**, 153 (1935); T. L. Gilbert, Phys. Rev. **100**, 1243 (1955).
[10] U. Gradmann, in *Handbook of Magnetic Materials*, edited by K. H. J. Buschow (Elsevier North-Holland, Amsterdam, 1993), Vol. 1.
[11] W. J. M. de Jonge, P. J. H. Bloemen, and F. J. A. den Broeder, in *Ultrathin Magnetic Structures*, edited by J. A. C. Bland and B. Heinrich (Springer, New York, 1994), Vol. 1, p. 65.
[12] B. C. Choi, M. Belov, W. K. Hiebert, G. K. Ballentine, and M. R. Freeman, Phys. Rev. Lett. **86**, 728 (2001).
[13] H. Katada, T. Shimatsu, I. Watanabe, H. Muraoka, Y. Nakamura, and Y. Sugita, IEEE Trans. Magn. **37**, 2334 (2001).
[14] C. M. Fu, P. C. Kao, M. S. Tsai, H. S. Hsu, C. C. Yu, and J. C. A. Huang, J. Magn. Magn. Mater. **239**, 17 (2002).
[15] R. Loloee, S. Urazhdin, W. P. Pratt, H. Geng, and M. A. Crimp, Appl. Phys. Lett. **84**, 2364 (2004).